CFD Modeling and Simulation in Materials Processing 2016
Edited by: Laurentiu Nastac, Lifeng Zhang, Brian G. Thomas, Miaoyong Zhu, Andreas Ludwig, Adrian S. Sabau, Koulis Pericleous, and Hervé Combeau
TMS (The Minerals, Metals & Materials Society), 2016

PERFORMANCE OPTIMIZATION AND EVALUATION OF A 3D CA-FVM MODEL FOR DENDRITIC GROWTH OF Fe-C ALLOY

Weiling Wang[1], Sen Luo[1,2], Miaoyong Zhu[1]

[1]School of Metallurgy, Northeastern University, Shenyang 110819, China
[2]Ansteel research institute of vanadium & titantium (iron & steel), Ansteel Corporation, Panzhihua 610031, China

Keywords: Dendritic growth, Fe-C alloy, 3D CA-FVM model, 3D block-correction technique, Parallelization.

Abstract

Because of the tremendous computational cost of 3D (three dimensional) calculation of the dendritic growth, the parallel approach and the block-correction technique (BCT) are adopted to improve the efficiency of codes. Meanwhile, the accuracy of the codes is evaluated by comparing the present prediction with the analytical solutions to the fluid flow problem, LGK analytical results and the experimental measured columnar dendritic morphology and secondary dendritic arm spacing (SDAS, λ_2). The results show that the parallel Jacobi code with once 2D iteration in 3D BCT is proved to be the most efficient one among the codes compiled in the present work, accordingly is employed to simulate the 3D dendritic growth of alloys. The calculated velocities agree well with the results from the analytical equations. The predicted steady growth velocities of the equiaxed dendritic tip of Fe-0.82wt%C alloy by the present CA model agree with the 3D LGK analytical model as the anisotropy parameter is 0.04. Moreover, the present CA model shows some capability to predict the columnar dendritic growth during the directional solidification process of Fe-1.48wt%C alloy.

Introduction

With the increasing demand for simulating the dendritic growth of alloys closer to the actual case, the numerical simulation by the deterministic models such as the phase field (PF) model and the front tracking (FT) model and the stochastic models such as the cellular automaton (CA) model has been extended from two dimensional (2D) domain to three dimensional (3D) domain.
As the additional dimension is introduced, the computational cost boosts up significantly, especially in consideration of the melt flow, which is the most serious problem confronted by the model developers. Therefore, the algorithm optimization and the parallel computation are usually employed to improve the computation efficiency. The simulation of the dendritic growth in 3D was firstly realized with the PF model [1]. At first, considering the importance of the solidification interface to dendritic evolution, the adaptive-mesh approach with the much finer meshes at the interface and coarser meshes at the remain domain was usually used to reduce the computational cost of 3D PF models during the simulation of the dendritic growth of pure materials [2, 3]. With the development of computers, the parallel 3D PF models based on the message-passing interface (MPI) library become dominant to predict the dendritic growth with a reasonable computational efficiency [4]. The fundamental of the parallel approach is that the task is divided into several subdomains which are assigned to different processors and calculated

L. Nastac et al. (Eds.), *CFD Modeling and Simulation in Materials Processing 2016*

separately, meanwhile its continuity is guaranteed by the process communication, that is, the MPI approach. Moreover, the combination of the adaptive-mesh and the parallelization approach are usually combined to further improve the computational efficiency of PF models [5]. Similarly, Al-Rawahi and Tryggvason [6] implemented the 3D FT model on parallel computers using the MPI approach. Zhao and coauthors [7-10] realized the parallelization of their 3D CA-FVM (cellular automaton-finite volume method) model with discrete linear equations being solved by 3D TDMA (tri-diagonal matrix algorithm) by using the MPI approach. However, compared with other algorithms such as Jacobi, TDMA is intrinsically with the serial characteristic. Therefore, Eshraghi et al. [11, 12] introduced the 3D lattice Boltzmann method (LBM) with the complete parallelism to deal with transport equations and extended the computational scale of the 3D CA-LBM model to 3.6 billion cells. Moreover, another advantage of LBM is that it can deal with the fluid flow in the discontinuous regions well, compared with traditional CFD (computational fluid dynamics) approaches. Recently, the graphic processing unit (GPU) has been used to accelerate the calculation of the 3D PF model in large scale domains [13]. For the traditional methods such as FDM (finite difference method) and FVM still used in the simulation of the dendritic growth [7-10], except for the parallelism, some acceleration algorithms for the calculation of discrete equations should be considered to obtain an acceptable computational cost. For example, the block-correction technique (BCT) [14] can promote the convergence of the iterations of linear equations by methods such as TDMA and Jacobi and has been applied in the investigation of dendritic growth under the melt flow in 2D with CA approach by present authors [15, 16]. Therefore, its application in 3D will be expected, as well as its combination with the parallelization of the codes. Additionally, the accuracy of the 3D codes should be concerned to ensure their capability in predicting the 3D dendritic growth of alloys. The models for the dendritic evolution are customarily tested through the comparisons of the steady dendritic tip parameters [17, 18], the qualitative dendritic morphology [18] and the dendritic arm spacing (DAS)[7, 9, 10] with analytic models and experimental results. Taking the advantage of the superiority of the FT model, Al-Rawahi and Tryggvason [6] tested their model and flow solvers with respect to the analytical solutions for the Stefan problem of a sphere and for the flow over a simple cubic array of spheres. Although this concept is very constructive and novel, comparisons with solutions of Stefan problems cannot be transplanted to the CA model. It is mainly ascribed to that the isothermal solidification interface in Stefan problems should be explicitly tracked to consider the release of solidification heat there, which cannot be realized in the CA model. As a result, Yin et al. [19] employed analytical solutions of pure thermal and solute diffusion to validate the heat transfer and solute diffusion solvers in 2D, however neglected the test of the flow solver.

A 3D CA-FVM model focusing on the 3D dendritic growth of high carbon Fe-based alloys was developed in the consideration of the improvement of the computational efficiency and the model capacity [20, 21]. Compared with other works with traditional transport models [7-9], the present work employed both the 3D BCT and the parallelism to save the computational cost. The present paper will give a brief introduction of the first part of the work involving mainly seeking for the most efficient code to deal with the designed problems and evaluating the capability of 3D CA-FVM model in solving the transport problem and the dendritic evolution.

Model Description

Governing Equations

The governing equations for the inter- and exter-dendritic flows are given by:

$$\nabla \cdot (\rho \boldsymbol{U}) = 0 \tag{1}$$

$$\rho \frac{\partial \boldsymbol{U}}{\partial t} + (\rho \boldsymbol{U}) \cdot \nabla (\boldsymbol{U}) = -\nabla p + \nabla \cdot (\mu \nabla (\boldsymbol{U})) \tag{2}$$

where $\boldsymbol{U}$ is velocity vector, (u, v, w), ρ is density, μ is viscosity, and p is the hydrostatic pressure. The governing equations of solute transport are given by:

$$\frac{\partial C_l}{\partial t} + (\boldsymbol{U}) \cdot \nabla C_l = D \cdot \nabla^2 C_l \tag{3}$$

$$\frac{\partial C_s}{\partial t} = D \cdot \nabla^2 C_s \tag{4}$$

where C_s and C_s are solute concentrations in solid and liquid phases, respectively, and D is diffusion coefficient, which is the mean value of solid diffusivity, D_s and liquid diffusivity, D_l according to the solid fraction, f_s.

The governing equation of the heat transport is expressed as follows:

$$\frac{\partial T}{\partial t} + \boldsymbol{U} \cdot \nabla T = \alpha \cdot \nabla^2 T + \frac{L}{c} \frac{\partial f_s}{\partial t} \tag{5}$$

where T is temperature, α is thermal diffusivity, which is the function of the thermal conductivity, λ and the specific heat capacity, c, and L is solidification latent heat.

The convergence of transport equations should satisfy Eqs. (6) and (7):

$$\mathrm{Max}\left[\frac{\zeta_{i,j,k}^{n+1} - \zeta_{i,j,k}^{n}}{\mathrm{CT}} \right] < \chi \tag{6}$$

$$\mathrm{CT} = \begin{cases} 1 & \zeta_{i,j,k}^{0} >= 1 \\ \zeta_{i,j,k}^{0} & \zeta_{i,j,k}^{0} < 1 \end{cases} \tag{7}$$

where ζ represents field variables, including u, v, w, T and C, ζ^0 is on behalf of initial values of those variables, n is iteration steps, χ is a number far less than unity, CT is a constant dependent on ζ^0, and (i, j, k) denotes the serial number of the CA cell.

The Neumann configuration is used to deal with the evolution of the state of the CA cell. Accordingly, as the interface cell become solid, it will capture the liquid cells among its first nearest cells as the interface cells. The solute redistribution at the interface is given by:

$$C_s^* = k_0 C_l^* \tag{8}$$

$$C_l^* = C_0 + \frac{1}{m_l} \left(T^* - T_l + \Gamma \cdot wmc \right) \tag{9}$$

where C_l^* and C_s^* are equilibrium solid and liquid solute concentrations at solidification interface, respectively, k_0 is the equilibrium partition coefficient of the solute, C_0 is the initial solute content in the modeling domain, T_l is the equilibrium liquidus temperature, m_l is the slope of liquidus line in the equilibrium phase diagram of the alloy, Γ is the Gibbs-Thomson coefficient of Fe-C alloy, and T^* is the interface temperature. *wmc* is expressed in Eq. (10) [18]:

$$wmc = (3\varepsilon - 1)\cdot\left(\partial_x n_x + \partial_y n_y + \partial_z n_z\right) - 48\varepsilon\cdot\left(n_x^2\cdot\partial_x n_x + n_y^2\cdot\partial_y n_y + n_z^2\cdot\partial_z n_z\right) + 12\varepsilon\cdot Q\cdot\left(\partial_x n_x + \partial_y n_y + \partial_z n_z\right) + 12\varepsilon\cdot\left(n_x\cdot\partial_x Q + n_y\cdot\partial_y Q + n_z\cdot\partial_z Q\right) \quad (10)$$

where ε is the anisotropic degree of the surface energy, (n_x, n_y, n_z) is unit normal vector of the interface and is calculated according to the first-order derivative of solid fraction, f_s, such as $n_x=\partial_x f_s/[(\partial_x f_s)^2+(\partial_y f_s)^2+(\partial_z f_s)^2]^{0.5}$. The parameter Q is denoted as $Q=n_x^4+n_y^4+n_z^4$.
The evolution of the solidification interface is governed by the solute balance there, as expressed in Eq. (11) [7-10, 15, 16, 20, 21].

$$v_n C_1^* (1-k_0) = D_s \frac{\partial C_s}{\partial \boldsymbol{n}}\bigg|^* - D_l \frac{\partial C_l}{\partial \boldsymbol{n}}\bigg|^* \quad (11)$$

where v_n is normal growth velocity of solidification interface. The solute balance along three axes is separately calculated [15, 16]. The related physical property parameters of high carbon Fe-C alloy are listed in the previous paper [15, 16, 20, 21].

Performance Optimization

According to the basic concept of FVM, the transport equations in 3D are discretized into a uniform form:

$$a_P\varphi_P - a_W\varphi_W - a_E\varphi_E - a_S\varphi_S - a_N\varphi_N - a_B\varphi_B - a_T\varphi_T = b_P \quad (12)$$

where a, b and φ are the coefficient, the constant term and the variable of the discrete equation, and P, W and E, T and B and N and S represent the present cell, its west and east neighboring cells along x axis, top and bottom nearest ones along z axis, and north and south nearest ones along y axis. The basic concept of the BCT is to introduce a mean modification value to ensure the complete conversation in the each iteration [14], as shown in Figure 1.
The Parallel Patterns Library (PPL) and the namespace Concurrency in Microsoft Visual Studio 2010 C++ are used to parallelize the codes. The codes are run on the server with 40 CPU cores.

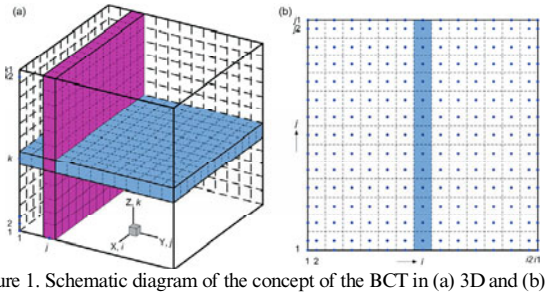

Figure 1. Schematic diagram of the concept of the BCT in (a) 3D and (b) 2D

Model Test

Transport Models

The computational efficiency of these codes is evaluated as they solve the designed melt flow problem, as illustrated in Figure 2(a) and (b). A fluid of the molten steel flows into the 201 μm ×

201 μm × 201 μm domain with the velocity of 0.001 m/s along x axis of at the left boundary, gets over the orthogonally arranged solid obstacles in the center of the domain and leaves at the right boundary, which belongs to the laminar category. The size of the block is 44 μm × 10 μm × 10 μm. Meanwhile, the domain is meshed into cells with the size of 1 μm × 1 μm × 1 μm. Except for the inlet and the outlet boundaries, other walls of the domain are symmetrical. The flow field at steady state is predicted with the SIMPLE algorithm. The number χ representing the convergence requirement is 0.001. As the 3D BCT is introduced, the computational cost of the serial TDMA code decreases from 92.62 h to 22.74 h, as shown in Figure 2(c). It is attributed to that the 3D BCT changes the convergence type of the iteration from the fluctuating one to a smooth one, according reduces the iteration steps. Subsequently, as the code is partially parallelized, the computational cost drops to 15.71 h. Such computational efficiency is still relatively high since TDMA is intrinsically serial. Therefore, Jacobi with much more parallel characteristic is employed to further improve the computational efficiency. The parallel Jacobi code with 3D BCT cost 8.67 h to get the convergence. According to the basic concept of BCT, the 2D iteration in 3D BCT is not necessarily required to be converged as the boundary condition is delivered into the computational domain. As the 2D iteration in 3D BCT in iterated once, the computational cost of the parallel Jacobi code reduces by 2.88 h. Moreover, as the compiling mode changes from debug to release, the computational cost of the parallel Jacobi code with once 2D iteration in 3D BCT reduces to an acceptable value, 2.60 h. Therefore, the parallel Jacobi code with once 2D iteration in 3D BCT is adopted to simulate the 3D dendritic growth of alloys in the present work.

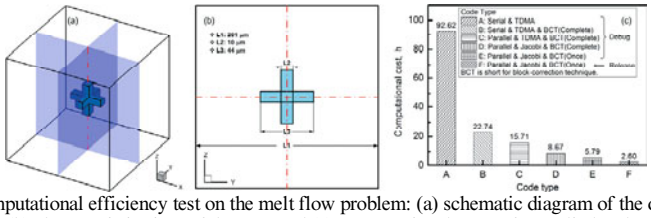

Figure 2. Computational efficiency test on the melt flow problem: (a) schematic diagram of the designed case, (b) characteristic sizes of the case and (c) computational costs of complied codes

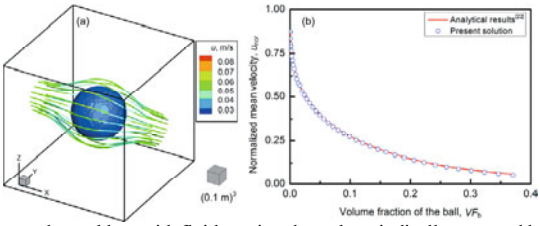

Figure. 3 Solution to the problem with fluid passing through periodically arranged balls: (a) the flow distribution around the solid ball and (b) comparison between the predicted normalized mean velocity, u_{nor} and the analytical results [22]

In order to evaluate the accuracy of the present fluid flow solver, the classical problem with flow passing through periodical arranged balls [22] is concerned. In order to impel the flow pass

through the gap between two adjacent balls with the size of L along x axis with the given average velocity $\overline{u}_0$, the driving force, that is, the pressure gradient β should be exerted. The normalized velocity u_{nor} representing the quantitative relationship between β and $\overline{u}_0$ changes with the volume fraction of the ball, VF_b. The fluid passes through the gap of 1.0 m between two adjacent balls with an average velocity of 0.1 m/s, as shown in Figure 3(a). The predicted functional relationship between u_{nor} and VF_b agrees well with the analytical result [22], as shown in Figure 3(b).

CA Model

The 3D LGK model without consideration of the thermal undercooling [17, 18] is adopted to evaluate the present CA-FVM model. The selection parameter of the dendritic tip, σ* used in the LGK model is determined to be 0.1273 corresponding to the anisotropy parameter of 0.04 according to the linearized solvability theory [23]. The cubic domain with the size of 201 μm × 201 μm × 201 μm meshed into (1 μm)^3 cells is used to simulate the single equiaxed dendritic growth of Fe-0.82wt%C alloy at the constant undercooling. The solute diffusion in solid phase is neglected in terms of the basic concept of the LGK mode. As the solidification time reaches the order of D/V^2 [18], the dendritic growth is assumed to be at steady state. Accordingly, the steady growth velocity and radius of the dendritic tip can be determined. Figure 4 shows the comparisons between the predicted steady growth velocity and radius of the dendritic tip and the analytical results as the undercooling changes from 3 K to 13 K. The predicted steady growth velocities of dendritic tip present good agreements with the LGK analytical results at the undercooling of 6-7 K. The steady tip radius is consistent with the analytical prediction at the undercooling of 6.5 K. Meanwhile, the difference between the prediction and the analytical data can be attributed to the mesh dependence of the CA model.

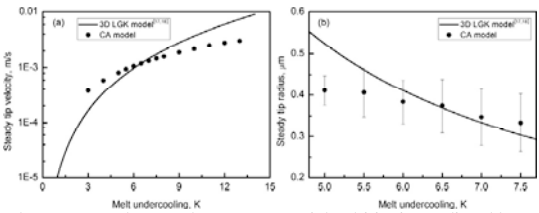

Figure. 4 Comparison between steady growth parameters of dendritic tip predicted by present CA model and the LGK analytical results: (a) the steady growth velocity and (b) the steady radius

Additionally, the unidirectional solidification processes of the high carbon steel presented by Jacobi and Schwerdtfeger [24] are adopted to evaluate the capability of present codes in predicting the columnar dendritic growth. The steel is simplified into Fe-1.48wt%C alloy. In the simulation, the nuclei are placed at the bottom domain according to the measured average primary dendritic arm spacing (PDAS, λ_1) [24] as listed in Table I. The cooling conditions are strictly in accordance with the experimental conditions with the given growth rate, R_d and the given temperature gradient, G, which are listed in Table I. Firstly, the columnar dendritic morphology of Fe-1.48wt%C at the cooling condition with R_d=0.51 m/h and G=5200 K/m (λ_1=540 μm) is predicted by the present CA-FVM model which agree with the experimental

result, as shown in Figure 5. The SDAS are measured as the columnar dendrites reach the top of the domain in the consideration of the dendritic coarsening and compared with the experimental measurements as listed in Table I. The predicted average SDASs shows some agreement with the experimental results, especially at R_d=0.51 m/h and G=7400 K/m.

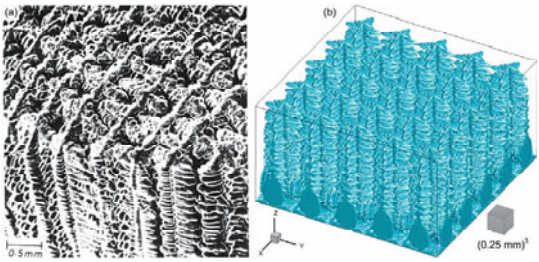

Figure. 5 Columnar dendritic morphology of Fe-1.48wt%C alloy during the unidirectional solidification: (a) the experimental observation [24] and (b) the predicted result

Table I Comparisons between the predicted SDASs and the experimental measurements[24]

R_d, m/h	G, K/m	$\lambda_{1,\,Mea}$, μm	$\lambda_{2,\,Mea}$, μm	$\lambda_{2,\,Cal}$, μm		
				MAX	MIN	AVE
0.25	5300	570	**150.0**	160.0	60.0	**110.0**
0.25	7000	370	**130.0**	170.0	75.0	**107.0**
0.51	5200	540	**110.0**	110.0	55.0	**77.0**
0.51	7400	320	**70.0**	90.0	45.0	**69.3**
0.75	8800	280	**80.0**	80.0	30.0	**52.0**

Conclusion

(1) With the introduction of the 3D BCT and the parallelism, the former serial TDMA code is gradually optimized to the parallel Jacobi code with once 2D iteration in 3D BCT with the computational cost reducing from 92.62 h to 5.79 h as it deals with the flow problem with the scale of 201^3. As the compile mode is changed from debug to release, the computational cost of this code become more acceptable. The solutions for the problem with the fluid passing through the gap between periodically arranged balls agree well with the analytical results.
(2) The predicted steady tip velocity and radius agree well with the LGK analytical model at the undercooling of 6-7 K. Moreover, the predicted columnar dendritic morphology of Fe-1.48wt%C alloy during the unidirectional solidification agrees with the experimental observation. The calculated SDASs agree with the experimental results, especially at the growth velocity of 0.51 m/h and the temperature gradient of 7400 K/m.

Acknowledgement

The authors sincerely acknowledge the financial support from National Natural Science Foundation of China No. 51404062 and Outstanding Talent Cultivation Project of Liaoning Province No. 2014029101 and Specialized Research Fund for the Doctoral Program of Higher Education of China No. 20130042120042.

References

1. A. Karma and W. J. Rappel, "Quantitative Phase-Field Modeling of Dendritic Growth in Two and Three Dimensions", *Physical review E*, 57 (4) (1998), 4323.
2. J. H. Jeong, N. Goldenfeld, and J. A. Dantzig, "Phase Field Model for Three-Dimensional Dendritic Growth with Fluid Flow", *Physical Review E*, 64 (4) (2001), 041602.
3. C. C. Chen and C. W. Lan, "Efficient Adaptive Three-Dimensional Phase-Field Simulation of Dendritic Crystal Growth From Various Supercoolings Using Rescaling", *Journal of Crystal Growth*, 311 (3) (2009), 702-706.
4. W. L. George and J. A. Warren, "A Parallel 3D Dendritic Growth Simulator Using the Phase-Field Method", *Journal of Computational Physics*, 177 (2) (2002), 264-283.
5. P. C. Bollada, P. K. Jimack, and A. M. Mullis, "An Adaptive Mesh Method for Phase-Field Simulation of Alloy Solidification in Three Dimensions", *IOP Conference Series: Materials Science and Engineering*, 84 (1) (2015), 012068.
6. N. Al-Rawahi and G. Tryggvason, "Numerical Simulation of Dendritic Solidification with Convection: Three-Dimensional Flow", *Journal of Computational Physics*, 194 (2) (2004), 677-696.
7. H.X. Jiang and J.Z. Zhao, "A Three-Dimensional Cellular Automaton Simulation for Dendritic Growth", *Acta Metallurgica Sinica*, 47 (9) (2011), 1099-1104.
8. X.F. Zhang and J.Z. Zhao, "Effect of Forced Flow on Three Dimensional Dendritic Growth of Al-Cu Alloys", *Acta Metallurgica Sinica*, 48 (5) (2012), 615-620.
9. X.F. Zhang, J.Z. Zhao, H.X. Jiang, et al., "A Three-Dimensional Cellular Automaton Model for Dendritic Growth in Multi-Component Alloys", *Acta Materialia*, 60 (5) (2012), 2249-2257.
10. X.F. Zhang and J.Z. Zhao, "Dendritic Microstructure Formation in A Directionally Solidified Al-11.6Cu-0.85Mg Alloy", *Journal of Crystal Growth*, 391 (2014), 52-58.
11. M. Eshraghi , S.D. Felicelli, and B. Jelinek, "Three Dimensional Simulation of Solutal Dendrite Growth Using Lattice Boltzmann and Cellular Automaton Methods", *Journal of Crystal Growth*, 354 (1) (2012), 129-134.
12. M. Eshraghi , B. Jelinek, and S.D. Felicelli, "Large-Scale Three-Dimensional Simulation of Dendritic Solidification Using Lattice Boltzmann Method", *JOM*, 67 (8) (2015), 1786-1792.
13. T. Takaki, "Phase-field Modeling and Simulations of Dendrite Growth", *ISIJ international*, 54 (2) (2014), 437-444.
14. Wenquan Tao, *Numerical Heat Transfer* (Xi'an: Xi'an Jiao Tong University Press, 2001), 280-283.
15. W.L. Wang, S. Luo, and M.Y. Zhu, "Numerical Simulation of Dendritic Growth of Continuously Cast High Carbon Steel", *Metallurgical and Materials Transactions A*, 46 (1) (2015), 396-406.
16. W.L. Wang, S. Luo, and M.Y. Zhu, "Dendritic Growth of High Carbon Iron-Based Alloy Under Constrained Melt Flow", *Computational Materials Science*, 95 (2014), 136-148.
17. J. Lipton, M. E. Glicksman, and W. Kurz, "Dendritic Growth into Undercooled Alloy Metals", *Materials Science and Engineering*, 65 (1) (1984), 57-63.
18. S.Y. Pan, M.F. Zhu, "A Three-Dimensional Sharp Interface Model for the Quantitative Simulation of Solutal Dendritic Growth", *Acta Materialia*, 58 (1) (2010), 340-352.
19. H. Yin, S.D. Felicelli, and L. Wang, "Simulation of A Dendritic Microstructure with the Lattice Boltzmann And Cellular Automaton Methods", *Acta Materialia*, 59 (8) 2011, 3124-3136.
20. W.L. Wang, S. Luo, and M.Y. Zhu, "Numerical Simulation of Three-Dimensional Dendritic Growth of Alloy Part I. Model Development and Test", *Metallurgical and Materials Transactions A*, (2015), Submitted.
21. W.L. Wang, S. Luo, and M.Y. Zhu, "Numerical Simulation of Three-Dimensional Dendritic Growth of Alloy Part II. Model Application to Fe-0.82wt%C alloy", *Metallurgical and Materials Transactions A*, (2015), Submitted.
22. A.S. Sangani and Acrivos A, "Slow Flow Through a Periodic Array of Spheres", *International Journal of Multiphase Flow*, 8 (4) (1982), 343-360.
23. A. Barbieri and J.S. Langer, "Predictions of Dendritic Growth Rates in the Linearized Solvability Theory", *Physical Review A*, 39 (10) (1989), 5314-5325.
24. H. Jacobi and K. Schwerdtfeger, "Dendrite Morphology of Steady State Unidirectionally Solidified Steel", *Metallurgical Transactions A*, 7 (6) (1976), 811-820.